Conventional and Contrast-enhanced Ultrasound Imaging in 2 Human Kidney Xenotransplant Recipients

Sylvain Bodard, MD, PhD,[1,2,3] Amirkasra Mojtahed, MD,[2,4] Madeleine Sertic, MD, BCh,[2,4,5] Theodore T. Pierce, MD, MPH,[2,4,5,6] Rory L. Cochran, MD, PhD,[2,4] Reece J. Goiffon, MD, PhD,[2,4,5] and Leonardo V. Riella, MD, PhD[1,2]

Background. Kidney xenotransplantation offers a promising novel solution to the global organ shortage, although the expected postoperative imaging characteristics remain undefined. **Methods.** We report the first application of longitudinal grayscale, color, and spectral Doppler ultrasound in 2 human recipients of genetically engineered porcine kidney xenografts. One recipient additionally underwent serial contrast-enhanced ultrasound to assess parenchymal perfusion. Imaging findings were correlated with serum creatinine trajectories and biopsy-proven rejection. **Results.** In both recipients, spectral Doppler abnormalities—including elevation in resistive index—preceded biopsy-confirmed T-cell–mediated rejection. Contrast-enhanced ultrasound in 1 recipient revealed delayed contrast enhancement that paralleled rejection and normalized with treatment. Neither graft demonstrated significant posttransplant growth, with observed changes in graft length remaining within the expected range for Yucatan miniature swine-derived kidneys. **Conclusions.** These findings provide the first preliminary ultrasound-based insights into kidney xenograft vascular dynamics and growth patterns, underscoring the potential of ultrasound as an essential tool for noninvasive monitoring of kidney xenotransplants.

(*Transplantation* 2025;00: 00–00).

INTRODUCTION

Kidney xenotransplantation recently transitioned from preclinical to early human studies, offering a potential solution to donor organ scarcity.[1-3] As a new strategy, long-term xenograft viability, functional integration, and optimal monitoring strategies are unknown.[4,5] Because xenotransplantation involves cross-species physiology, ultrasound findings may differ from those in allotransplantation because of species-specific differences in vascular architecture, immune-mediated injury patterns, neurohormonal differences (eg, incompatibility of the renin-angiotensin-aldosterone system), and microvascular response to rejection. These distinctions highlight the need to characterize imaging correlates specifically in the xenotransplant setting.

Ultrasound, including B-mode, color Doppler, spectral Doppler, and contrast-enhanced ultrasound (CEUS), is the primary technique to assess graft perfusion, vascular and nonvascular complications, and rejection.[6] Utility of ultrasound for kidney xenotransplantation remains unexplored.[7]

Graft size stability and porcine xenograft growth potential in humans is also undercharacterized.[8] While porcine-to-nonhuman primate kidney xenotransplantation studies show 30% increase in graft long-axis length within 2 wk, possibly increasing risk of ischemia via growth-induced compartment syndrome,[9] studies using genetically modified miniature swine donor kidneys demonstrated minimal posttransplant growth.[10] Whether these findings will apply to human recipients remains unknown.

Received 24 April 2025. Revision received 21 August 2025.

Accepted 23 August 2025.

[1] Center for Transplantation Sciences, Department of Surgery, Massachusetts General Hospital, Boston, MA.

[2] Harvard Medical School, Boston, MA.

[3] Sorbonne Université, CNRS, INSERM, Laboratoire d'Imagerie Biomédicale, Paris, France.

[4] Department of Radiology, Massachusetts General Hospital, Boston, MA.

[5] Center for Ultrasound Research & Translation, Massachusetts General Hospital, Boston, MA.

[6] Department of Radiology, Brigham and Women's Hospital, Boston, MA.

The authors declare no funding or conflicts of interest.

S.B., A.M., M.S., T.T.P., R.G., and L.V.R. participated in research design. S.B., A.M., M.S., T.T.P., R.J.G., and L.V.R. participated in investigation. S.B., A.M., M.S., T.T.P., R.C., R.J.G., and L.V.R. participated in data analysis. S.B. participated in writing—original draft. S.B., A.M., M.S., T.T.P., R.C., R.J.G., and L.V.R. participated in writing—review and editing. L.V.R. participated in supervision.

Visual abstract is available online at doi.org/10.1097/TP.0000000000005538.

Supplemental digital content (SDC) is available for this article. Direct URL citations appear in the printed text, and links to the digital files are provided in the HTML text of this article on the journal's Web site (www.transplantjournal.com).

Correspondence: Sylvain Bodard, MD, PhD, and Leonardo V. Riella, MD, PhD, Center for Transplantation Sciences, Department of Surgery, Massachusetts General Hospital, Harvard Medical School, 55 Fruit St, White 546C, Boston, MA 02114. (sylvain.bodard@aphp.fr; lriella@mgh.harvard.edu).

ISSN: 0041-1337/20/0000-00

DOI: 10.1097/TP.0000000000005538

This case series presents the first longitudinal ultrasound assessment of 2 kidney xenograft recipients reporting trends in xenograft size and vascular flow and, for 1 patient, CEUS assessment of microvascular perfusion. These findings establish foundational imaging protocols and strategies in kidney xenotransplantation monitoring.

MATERIALS AND METHODS

This case series includes 2 recipients of EGEN-2784 gene-edited porcine kidney xenografts from Yucatan miniature swine. These donor pigs underwent extensive genetic engineering to enhance xenograft compatibility and safety. This included a triple knockout of key xenoantigens (GGTA1, CMAH, and B4GALNT2) to prevent hyperacute rejection; insertion of 7 human transgenes (hCD46, hCD55, hEPCR, hTHBD, hCD47, HMOX1, and hTNFAIP3) aimed at complement regulation, coagulation control, immune modulation, and inflammation reduction; and inactivation of all porcine endogenous retroviruses to mitigate the theoretical risk of cross-species viral transmission.[3] The donor pig for recipient 1 was 12 mo old, weighed 74 kg, and the kidney measured 10.3 cm in length at the time of procurement. The donor pig for recipient 2 was 17 mo old, weighed 70 kg, and the kidney measured 10.9 cm in length.

Recipient 1 was a 62-y-old male (body mass index 34) with end-stage renal disease because of diabetic nephropathy and hypertension, exacerbated by nephrectomy for renal cell carcinoma and a failed prior kidney transplant.[3] Recipient 2 was a 66-y-old male (body mass index 30) with end-stage renal disease because of diabetic nephropathy. Both patients were on hemodialysis before transplantation and had type 2 diabetes, hypertension, peripheral vascular disease, and coronary artery disease.

The immunosuppressive regimen for recipient 1 consisted of induction therapy with rituximab, rabbit antithymocyte globulin (Thymoglobulin), ravulizumab, and steroids, followed by maintenance therapy with anti-CD154 antibody (Tegoprubart), tacrolimus, mycophenolic acid (Myfortic), and low-dose prednisone. Recipient 2 received rituximab, rabbit antithymocyte globulin, pegcetacoplan, and steroids for induction, followed by maintenance with anti-CD154 antibody, tacrolimus, mycophenolic acid, and low-dose prednisone. Immunosuppressive dosing was adjusted based on clinical progression, imaging findings, and biopsy results.

Ultrasound with B-mode and Doppler imaging was performed immediately after surgery and every 1–2 d using a GE Logiq E10 (GE Healthcare, Chicago, IL) with a C1–C6 curved array transducer. Standard clinical evaluation included B-mode assessment of renal morphology and a long-axis measurement. Spectral Doppler waveforms, peak systolic and end-diastolic velocities, and resistive indices (RIs) were obtained at the main renal artery, arterial anastomosis, and 3 arcuate arteries. Flow velocity minima and maxima were measured in the renal vein. In recipient 2, CEUS was performed weekly to assess microvascular perfusion. Imaging was conducted alternately by experienced sonographers and radiologists with >5 y of experience.

Imaging findings were correlated with the clinical course and biopsy histopathology as assessed by clinical pathologists. Perfusion was assessed by CEUS enhancement patterns and dynamics. Kidney length was plotted over time. This study was conducted with approval from the Institutional Review Board at Massachusetts General Hospital, under Institutional Review Board protocol numbers (2023P003631 recipient 1) and (2024P003475 recipient 2).

RESULTS

Grayscale and Doppler Ultrasound

Recipient 1

Prerejection Findings

Baseline ultrasound on posttransplant day 0 demonstrated normal renal architecture, homogeneous cortical echogenicity, and an RI of 0.63 (0.60–0.68). RI remained stable until day 3. The scans showed no graft swelling, vascular deficits, parenchymal abnormalities, or hydronephrosis (Figure 1A). Creatinine trended down from 8.9 mg/dL on the day of transplant to 2.6 mg/dL by day 3.

During Rejection

From day 3, vascular resistance progressively increased, RI reaching 0.83 (0.78–0.86) by day 13 driven by reduced diastolic flow (Figure 1B). Grayscale ultrasound showed a swollen appearance with renal sinus effacement, loss of lobulation and corticomedullary dedifferentiation because of edema (Figure 1B). Following a rapid and marked increase in serum creatinine (creatinine rose from 2.7 mg/L on day 7 to 3.9 mg/dL on day 8), a biopsy on day 8 confirmed severe acute T-cell–mediated rejection (Banff type 2a), prompting the initiation of antirejection therapy (high-dose steroids, pegcetacoplan and thymoglobulin).

Posttreatment (Following Rejection Therapy)

After antirejection therapy began on day 8, RI normalized by day 16 and remained stable through day 41 (0.63 [0.56–0.72]) (Figure 1C and D) with a creatinine of 2.5 mg/dL that further trended down to 1.8 mg/dL by day 26 remaining between 1.5 and 1.8 mg/dL subsequently. Grayscale abnormalities resolved (Figure 1C). A biopsy on day 30 confirmed the resolution of rejection.

The patient died on day 52 because of ventricular dysrhythmia secondary to diabetic cardiomyopathy and severe coronary artery disease. The kidney xenograft at autopsy did not reveal any rejection.

Recipient 2

Baseline Doppler Ultrasound

The initial posttransplant day 0 ultrasound demonstrated homogeneous renal parenchyma with normal cortical echogenicity, a borderline elevated RI of 0.76 (0.61–0.85), and no fluid collections or hydronephrosis (**Figure S1A, SDC**, https://links.lww.com/TP/D307).

Longitudinal Doppler Findings

Between days 1–6, RI values remained stable at 0.78 (0.72–0.81) with a creatinine that trended down from 7.1 mg/dL on day of transplant to 1.2 mg/dL on day 6. From day 6, RI progressively increased to 0.83 (0.78–0.85) on day 12 (**Figure S1B, SDC**, https://links.lww.com/TP/

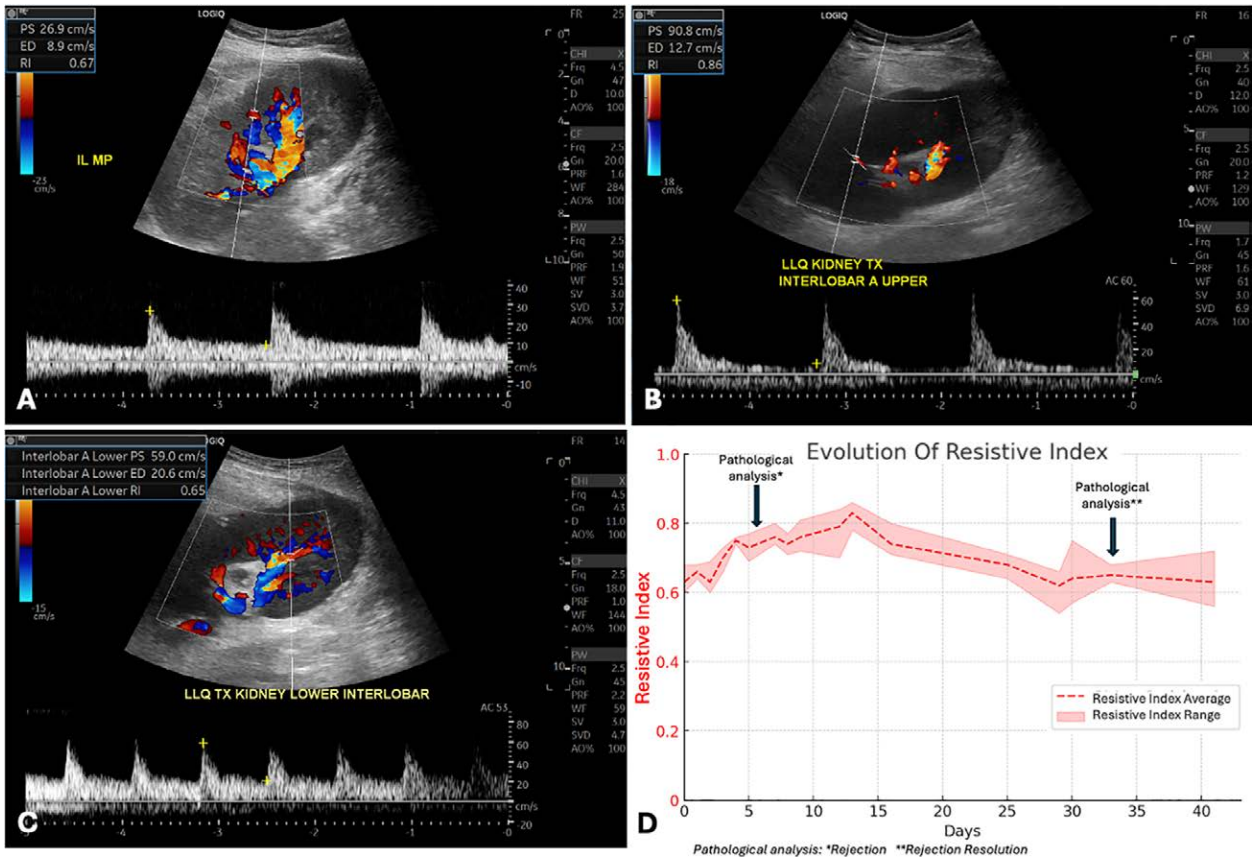

FIGURE 1. Spectral Doppler assessment of kidney xenograft in a 62-y-old male with end-stage renal disease (ESRD) secondary to diabetic nephropathy and hypertension, with a history of failed prior kidney transplant. A, Spectral Doppler evaluation (day 1) before rejection shows a normal arcuate arterial waveform with normal RI (RI = 0.67). B, Spectral Doppler assessment during severe rejection (day 13) reveals diminished arcuate artery diastolic flow and elevated RI (RI = 0.86), indicating impaired perfusion. C, Spectral Doppler evaluation after antirejection therapy (day 30) demonstrates arterial waveform normalization and normal RI (RI = 0.65). D, RI is plotted over time, highlighting the RI increase during rejection and subsequent normalization following treatment. ED, end diastolic velocity; IL, interlobar artery; LLQ, left lower quadrant; MP, midpole; PS, peak systolic velocity; RI, resistive index; TX, transplant.

D307) despite stable creatinine at 1.3 mg/dL. Grayscale ultrasound showed a swollen appearance with renal sinus effacement, loss of lobulation and corticomedullary dedifferentiation because of edema and graft enlargement, while color Doppler imaging was unchanged (**Figure S1B, SDC**, https://links.lww.com/TP/D307).

Mildly increased serum creatinine prompted a biopsy on day 14 (from 1.4 mg/dL on day 12 to 1.9 mg/dL on day 14), revealing acute T-cell–mediated rejection (Banff type 2a), leading to the initiation of antirejection therapy (high-dose steroids and thymoglobulin).

After antirejection therapy began, RI returned to borderline elevated values 0.73 (0.72–0.73) by day 21 with normalization of creatinine to 1.01 mg/dL (**Figure S1C** and **D, SDC**, https://links.lww.com/TP/D307). Grayscale abnormalities resolved (**Figure S1C, SDC**, https://links.lww.com/TP/D307). Three subsequent biopsies confirmed resolution of rejection, although an elevation of creatinine occurred in the setting of acute kidney injury attributed to vancomycin toxicity on day 74 posttransplant, when RI values markedly increased to 0.93 (0.92–0.93). Following discontinuation of vancomycin and supportive management, renal function progressively improved and RI values returned to baseline, paralleling normalization of serum creatinine levels (**Figure S1D, SDC**, https://links.lww.com/TP/D307).

Longitudinal Graft Size

The first xenograft length from recipient 1 measured between 10.4 and 10.9 cm during the first 3 d posttransplantation (Figure 2A) and increased during a histologically confirmed episode of rejection (Figure 2B) (see below), reaching 13.3 cm (+22%) by day 25. Subsequently, the graft size gradually decreased and stabilized at 12.6 cm (+17%) by day 41 (Figure 2C), indicating an overall modest increase in xenograft size.

The second xenograft measured 11.07 cm on the initial posttransplant ultrasound (Figure 2D). Serial ultrasound measurements showed a slight increase in xenograft size over time, reaching 12.2 cm (+10%) by day 77 posttransplant (Figure 2E), with stability over time (Figure 2F).

CEUS Findings

Three CEUS examinations were performed on recipient 2 using sulfur hexafluoride lipid type A microspheres (LUMASON, Bracco, Italy), followed by a 10 mL saline flush. The technique was modified in real-time by experienced radiologists, with doses ranging from 0.75 to 2.0 mL to allow for optimal evaluation of graft perfusion.

The first CEUS (day 6) showed homogeneous cortical enhancement, with no areas of reduced perfusion. Contrast arrival time and enhancement remained within

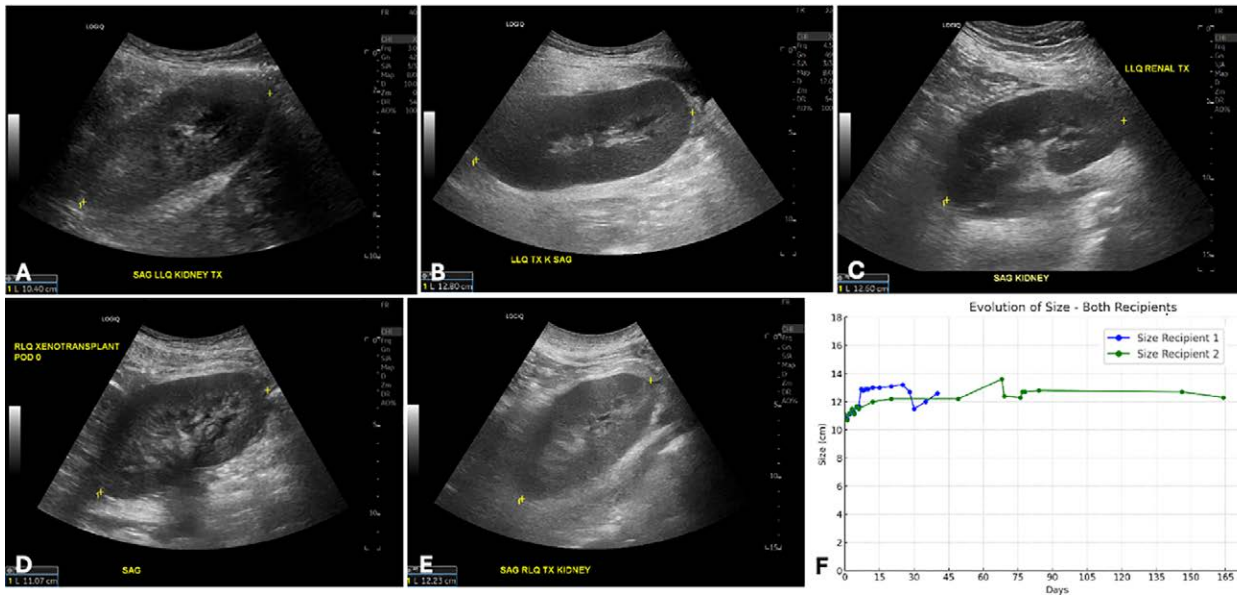

FIGURE 2. Temporal changes in kidney xenograft size. Grayscale ultrasound images of the transplanted kidney in recipient 1 on day 0 (10.40 cm; A), day 8 (12.80 cm; B), and day 41 (12.6 cm; C). Grayscale ultrasound images of the transplanted kidney in recipient 2 on day 0 (11.07 cm; D) and on day 21 (12.23 cm; E). F, Graph illustrating a slight overall increase in xenograft sizes over time. LLQ, left lower quadrant; POD, postoperative day; RLQ, right lower quadrant; SAG, sagittal; TX, transplant.

the expected range, with no qualitative microvascular perfusion abnormalities, suggesting preserved graft perfusion and stable hemodynamics (Figure 3).

The second CEUS (day 12; data not shown) revealed a slight delay in contrast arrival (18 versus 10 s) and cortical phase (20 versus 15 s) without major microvascular perfusion abnormalities, temporally correlating with biopsy-confirmed cellular rejection on day 14. The third CEUS (day 21) showed normalized microvascular perfusion (**Figure S2, SDC**, https://links.lww.com/TP/D307).

DISCUSSION

This case series, the first ultrasound-based assessment of human kidney xenografts, provides critical insights into their perfusion dynamics and structural stability. Spectral Doppler ultrasound detected increased RI and reduced diastolic flow preceding clinical rejection, while RI otherwise remained stable and within the normal range, suggesting good vessel compliance. CEUS in recipient 2 demonstrated normal enhancement during the initial rejection-free period and a slight delay in enhancement at the rejection onset. Serial graft length measurements showed only a slight increase over time.

Doppler findings during both rejection-free and rejection periods closely mirrored those in human kidney allografts.[11] Increased RI and reduced diastolic flow met established Doppler criteria for acute rejection in allotransplantation.[12,13] Other signs, including sudden graft swelling, echogenicity changes, and corticomedullary dedifferentiation, further support rejection.[6] However, it is important to note that an elevated RI is not specific for rejection and may also reflect other causes of acute kidney injury, such as drug-induced nephrotoxicity, vascular compromise, or hemodynamic alterations, underscoring the need for integration with biopsy and clinical context. Taken together, these findings support ultrasound as a noninvasive assessment technique for early kidney xenotransplant rejection while highlighting the importance of careful interpretation.

CEUS is a valuable tool in renal allotransplant perfusion assessment.[14] Stable, homogeneous cortical enhancement during the nonrejection period and slightly delayed enhancement in early rejection is consistent with allograft findings.[14] This suggests that CEUS may be a useful adjunct in diagnosing xenograft rejection. Although CEUS did not provide additional diagnostic information beyond Doppler ultrasound in our case of acute T-cell–mediated rejection, its inclusion was justified given its superior sensitivity and specificity for detecting other graft complications—such as infarction, cortical perfusion defects, or vascular thrombosis—which were not present in our patients but could arise in future clinical scenarios.

Another key finding was a modest posttransplant growth in porcine kidneys in this case series. Although Qi et al[9] described a 32% increase in kidney length within 16 d in a porcine-to-nonhuman primate model using a porcine kidney from a Bama miniature pig, and other reports of xenograft growth ranging from a 2-fold to 3-fold increase in xenograft volume or a doubling of length[15-17] using porcine kidneys from large white pigs and National Institutes of Health miniature swine, Firl et al[10] observed minimal posttransplant growth—~8% increase in length per year—in preclinical studies using Yucatan miniature swine donor kidneys with extensive genetic modifications. Our study, using the same donor pigs as Firl et al[10] showed similar findings over a shorter observation period, supporting the feasibility of long-term xenograft viability without disproportionate enlargement. While our findings suggest only modest early graft enlargement, we acknowledge the short follow-up period limits any definitive conclusions regarding long-term growth patterns or clinical implications. Future studies with extended surveillance will be necessary to assess the trajectory and relevance of xenograft size evolution.

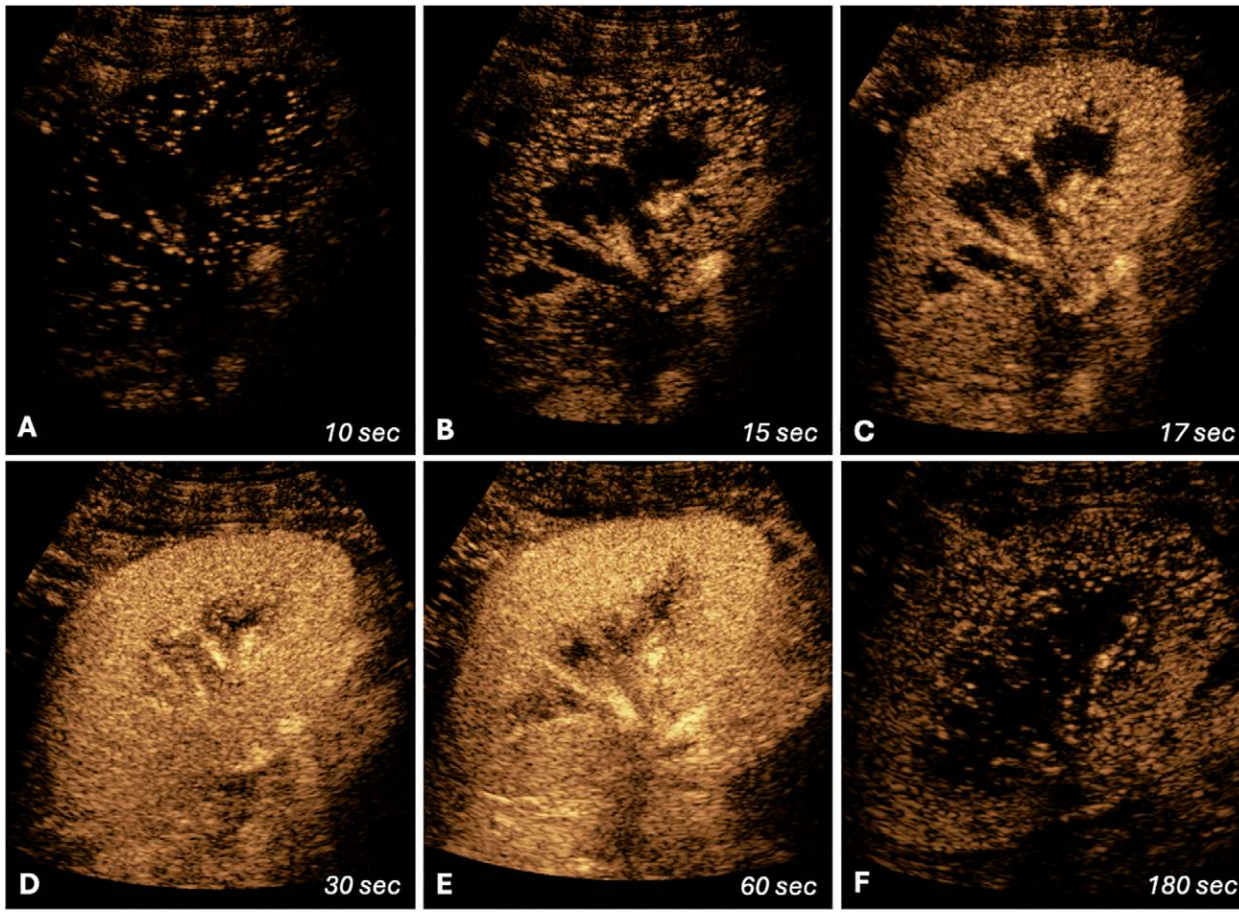

FIGURE 3. Normal contrast-enhanced ultrasound (CEUS) findings in recipient 2 during no rejection (day 6). A, Contrast arrival phase (at 10 s): initial appearance of contrast in the vasculature. B, Cortical phase (at 15 s): contrast enhancement of the renal cortex at the expected time. C and D, Early parenchymal phase (at 17 and 30 s): expected progressive contrast filling within the renal parenchyma. E, Late parenchymal phase (at 60 s): homogeneous perfusion of the renal parenchyma without defects or heterogeneity. F, Delayed phase (180 s): normal gradual washout of contrast from the parenchyma.

A slight increase in allograft size is common, reflects adaptation to hyperfiltration, and is associated with improved long-term survival, whereas decreased size during the first post-transplant year can indicate graft dysfunction. These changes depend on multiple factors including donor and recipient age, graft-to-recipient size ratio, and time since transplantation,[18,19] with ultrasound assessment showing high reproducibility.[20]

While no xenotransplantation-specific imaging features were identified in our cases, the similarity of Doppler and CEUS findings to established allograft rejection patterns suggests that existing imaging frameworks may be applicable to early xenograft monitoring. Further research is needed to explore whether specific pathophysiologic features—such as antibody-mediated rejection or microvascular thrombosis—may yield distinct imaging signatures in larger xenograft cohorts. Future studies should investigate CEUS in xenotransplantation, particularly during confirmed rejection, to evaluate its role in detecting microvascular injury and differentiating other complications, such as acute tubular necrosis, vascular thrombosis, or antibody-mediated rejection. Larger cohorts with extended follow-up are necessary to confirm the long-term xenograft growth patterns and stability of perfusion while integrating imaging with molecular and histopathologic analyses may provide further insights into xenograft adaptation in human recipients.

In conclusion, this is the first report of longitudinal ultrasound imaging in human kidney xenotransplantation from genetically edited miniature swine donors. Spectral Doppler changes correlated with acute rejection, while CEUS enabled detailed perfusion assessment. Serial ultrasound measurements showed no significant xenograft growth, addressing a key concern in the field. These findings underscore value of ultrasound in real-time, noninvasive xenograft monitoring.

ACKNOWLEDGMENTS

The authors thank eGenesis, the Philippe Foundation, L'Institut Servier, and the French Society of Radiology for their support.

REFERENCES

1. Riella LV. Xenotransplantation: the future is here. *J Am Soc Nephrol*. 2025;36:305–307.
2. Anand RP, Layer JV, Heja D, et al. Design and testing of a humanized porcine donor for xenotransplantation. *Nature*. 2023;622:393–401.
3. Kawai T, Williams WW, Elias N, et al. Xenotransplantation of a porcine kidney for end-stage kidney disease. *N Engl J Med*. 2025;392:1933–1940.
4. Locke JE, Kumar V, Anderson D, et al. Normal graft function after pig-to-human kidney xenotransplant. *JAMA Surgery*. 2023;158:1106–1108.

5. Montgomery RA, Stern JM, Lonze BE, et al. Results of two cases of pig-to-human kidney xenotransplantation. *N Engl J Med*. 2022;386:1889–1898.
6. Volkan-Salanci B, Erbas B. Imaging in renal transplants: an update. *Semin Nucl Med*. 2021;51:364–379.
7. Tector AJ, Adams AB, Tector M. Current status of renal xenotransplantation and next steps. *Kidney360*. 2022;4:278–284.
8. Pan W, Zhang W, Zheng B, et al. Cellular dynamics in pig-to-human kidney xenotransplantation. *Med*. 2024;5:1016–1029.e4.
9. Qi R, Ma S, Han S, et al. Intensive surveillance of porcine-rhesus kidney xenotransplant using different ultrasound techniques. *Xenotransplantation*. 2024;31:e12873.
10. Firl DJ, Lassiter G, Hirose T, et al. Clinical and molecular correlation defines activity of physiological pathways in life-sustaining kidney xenotransplantation. *Nat Commun*. 2023;14:3022.
11. Ghonge NP, Goyal N, Vohra S, et al. Renal transplant evaluation: multimodality imaging of post-transplant complications. *Br J Radiol*. 2021;94:20201253.
12. Mehrsai A, Salem S, Ahmadi H, et al. Role of resistive index measurement in diagnosis of acute rejection episodes following successful kidney transplantation. *Transplant Proc*. 2009;41:2805–2807.
13. Chanta G, Pattin M, Bozzo R, et al. Resistive index of renal grafts: its relation to systemic and renal vascular factors. *Transplantation*. 2018;102:S559.
14. Fernández T, Sebastià C, Paño B, et al. Contrast-enhanced US in renal transplant complications: overview and imaging features. *Radiographics*. 2024;44:e230182.
15. Cooper DKC, Hara H, Iwase H, et al. Clinical pig kidney xenotransplantation: how close are we? *J Am Soc Nephrol*. 2020;31:12–21.
16. Iwase H, Hara H, Ezzelarab M, et al. Immunological and physiological observations in baboons with life-supporting genetically engineered pig kidney grafts. *Xenotransplantation*. 2017;24:10.1111/xen.12293.
17. Tanabe T, Watanabe H, Shah JA, et al. Role of intrinsic (graft) versus extrinsic (host) factors in the growth of transplanted organs following allogeneic and xenogeneic transplantation. *Am J Transplant*. 2017;17:1778–1790.
18. Černe S, Arnol M, Kandus A, et al. Decrease in 1-year kidney graft size predicts inferior outcomes after deceased donor kidney transplantation. *Transplantation*. 2016;100:1759–1766.
19. Kostakis ID, Karydis N, Kassimatis T, et al. The implications of donor-recipient size mismatch in renal transplantation. *J Nephrol*. 2021;34:2037–2051.
20. Mancini M, Daniele S, Raffio T, et al. Intra and interobserver variability of renal allograft ultrasound volume and resistive index measurements. *La Radiologia Medica*. 2005;109:385–394.